

Cosmic Ray diffusion near the Bohm limit in the Cassiopeia A supernova remnant

M. D. Stage

*Five College Astronomy Department, University of Massachusetts
710 North Pleasant Street, Amherst, MA, 01003-9305*

and

G. E. Allen, J. C. Houck, and J. E. Davis

*MIT, Kavli Institute for Astrophysics and Space Research,
77 Massachusetts Avenue, Cambridge, MA, 02139-4307*

June 13, 2022

Supernova remnants (SNRs) are believed to be the primary location of the acceleration of Galactic cosmic rays, via diffusive shock (Fermi) acceleration. Despite considerable theoretical work the precise details are still unknown, in part because of the difficulty in directly observing nucleons that are accelerated to TeV energies in, and affect the structure of, the SNR shocks. However, for the last ten years, X-ray observatories *ASCA*, and more recently *Chandra*, *XMM-Newton*, and *Suzaku* have made it possible to image the synchrotron emission at keV energies produced by cosmic-ray *electrons* accelerated in the SNR shocks. In this article, we describe a spatially-resolved spectroscopic analysis of *Chandra* observations of the Galactic SNR Cassiopeia A to map the cutoff frequencies of electrons accelerated in the forward shock. We set upper limits on the diffusion coefficient and find locations where particles appear to be accelerated nearly as fast as theoretically possible (the Bohm limit).

Supernova remnants (SNRs) have been established as the leading candidate for the acceleration of cosmic rays.[1][2] It has been shown that the mechanism of diffusive shock acceleration in SNR shocks coupled with some understanding of Galactic transport effects can in theory produce the observed power-law spectrum of cosmic rays.[3]-[10]. This model works at least up to the “knee” of the cosmic ray spectrum near 5×10^{15} eV, and possibly

all the way to the “ankle” near 3×10^{18} eV.[11] The charged particles scatter off of irregularities in the magnetic field, increasing their momentum by a fraction of the shock velocity v/c with each round-trip shock crossing.[11] Theoretical work in the last several years has suggested that the process is significantly nonlinear.[10]-[15] Higher energy particles have larger diffusion lengths and therefore sample a greater change in velocity and compression ratio across the shock than lower energy particles. This effect introduces a decrease in the particle distribution’s spectral index and a flattening of the spectrum with increasing energy.[10] A smoothing effect on the structure of the shock results, predominantly caused by the ions; electrons are almost “test particles.” At high energies the electron spectrum is expected to have the same (curved) spectral shape as the proton spectrum.[10]

This correspondence of electron and proton spectra is significant because it is extremely difficult to directly observe the acceleration of cosmic-ray protons in SNR shocks. Their presence is inferred indirectly by detecting π^0 decay γ -rays produced from collisions of the cosmic rays with gas particles in the ambient medium. Atmospheric Cerenkov telescopes have observed gamma rays from some supernovae: Cas A with HEGRA[16][17], RX J1713.7-3946 (G347.3-0.5) with CANGAROO[18][19] and HESS[20], RX J0852.0-4622 with HESS[21] and CANGAROO-II[22], and G 0.9+0.1 with HESS[23]. Current technology limits the spatial resolution of these instruments to arcminutes and remnants the size of Cas A may appear point-like. In addition, TeV gamma rays can also be produced by inverse-Compton scattering of cosmic microwave background photons with the accelerated cosmic-ray electrons in SNRs. Consequently, it is difficult to precisely and unambiguously image proton and ion acceleration in the SNR. In contrast, the electrons which are accelerated to TeV energies produce synchrotron radiation at keV energies which is relatively easily imaged at arcsecond resolution. The electrons are not expected to be accelerated all the way to “knee” energies, as at some point the synchrotron losses equal the accelerative gains on shock crossing and the spectrum cuts off. However, it is still possible to set a lower limit on the efficiency of the acceleration.

An analysis of *ASCA* observations of SN 1006 provided the first evidence of X-ray synchrotron emission in an SNR.[24]. The approximately arcsecond spatial resolution over much of the energy band (0.5 - 10 keV) of the *Chandra* High Resolution Mirror Assembly—the best of any X-ray telescope which has flown[25] —has enabled detailed studies. For example, Lazendic et al.[26] studied *Chandra* observations of G347.3-0.5 to localize cosmic ray acceleration in filaments. Since the X-ray spectra of the youngest Galactic supernova remnants (Cas A, Tycho, and Kepler) are dominated by thermal emission,

the ability to spatially resolve the nonthermal contribution is especially important. Using *Chandra* observations, Warren et al.[27] demonstrated that acceleration in Tycho occurs at the forward shock.

Chandra's Advanced CCD Imaging Spectrometer's (ACIS) spectral resolution ($E/\Delta E \approx 10-60$) allows extraction of the spectrum of the emission. The combined capabilities of the mirror and CCDs allows us to determine if a nonthermal spectrum is present and where it is located. We:

1) developed a method to precisely identify the regions primarily radiating nonthermal X-ray synchrotron emission in a remnant dominated by thermal X-ray radiation from supernova ejecta;

2) fit the spectra of thousands of individual regions dominated by non-thermal emission in Cas A with a realistic synchrotron model, to map the synchrotron cut-off frequency around the outer shock;

3) determined the ratio of the estimated upper limit on the diffusion coefficient, $\bar{\kappa}$, in each region to the Bohm coefficient, κ_B , and thereby mapped the lower limit of the efficiency of acceleration in a SNR. In several areas, diffusion appears to be occurring near the Bohm limit. The maximum efficiency occurs in the northeast outer shock, just to the side of the jet, where $\bar{\kappa}/\kappa_B \leq 2.1$.

Mapping the spectral properties of the Cas A SNR

Exploiting the full capabilities of *Chandra*'s spatial resolution, ACIS's spectral resolution, the scripting functionality of the Interactive Spectral Interpretation System (ISIS)[28], and distributed computation, we produced high quality, high resolution maps of the spectral parameters of the remnant. We used direct spectral fitting, not energy selection methods. This process allowed us to map parameters such as temperature and interstellar absorption column, which is not possible with other methods.

We used the nine individual pointings from the million second observation of Cas A[29] and two additional archival observations to take the deepest look to date at a SNR with *Chandra*. Figure 1 shows a combined counts image color-coded by energy. To perform the spatially-resolved spectral analysis, we divided the sky around Cas A into a square grid of sky-coordinate region centers separated by approximately $1''$ (2 ACIS pixels). Cas A was covered by 104,393 regions. Each region was adaptively sized to contain a minimum of 10,000 counts. The region sizes ranged from $1'' \times 1''$ to $7'' \times 7''$ on source. Regions were allowed to overlap; therefore, fits to regions larger than $1'' \times 1''$ are not independent.

The position and roll angle of Cas A on the CCD varies in the eleven

pointings. We applied standard processing and filtering to the data for each pointing and then some custom techniques.[30] We re-projected the data to a common sky-coordinate plane, but maintained separate files for each pointing. To speed the later extraction of spectra, we histogrammed the spectral data and determined the mean chip coordinates and the exposure time for each sky location. This allowed us to separate the slowly varying effect of the effective area, which we calculated on a 32 pixel by 32 pixel grid, and the quickly varying effect of bad pixels and the exposure time, which we calculated on a pixel to pixel basis. Since our modified effective area depends only on chip location, we used one library of the effective area function for all of the pointings corresponding to a given observation epoch. Similarly, we pre-computed a library of energy response matrices on the same 32 pixel by 32 pixel grid.

Using ISIS, the same spectral model was fit jointly to the set of eleven spectra for each region. Each spectrum was associated with its own effective exposure, response functions, and optionally, background spectrum extracted from the same pointing. The background spectrum was not subtracted from the source spectrum, but was instead added to the model. The background is dominated by photons from Cas A in the wings of the point spread function of the telescope and in the CCD readout streak. For computational simplicity, the background for every source spectrum was drawn from the same representative sky region.

The analyses were performed in two phases. In Phase 1, we used a simple fitting function of fifteen Gaussian lines for specific O, Ne, Mg, Si, S, Ar, Ca, Ti and Fe line complexes (representing He-like K_α for all, He-like K_β for Si and S, H-like K_α for Si, and L lines for multiple Fe ions); an interstellar absorption column; and a bremsstrahlung continuum. This particular model was fit without background spectra (because it fits the background) to the 104,393 regions covering the entire remnant. The joint best-fit spectral parameters were recorded for each region and used to create FITS images of the spectral properties. Figure 2 shows the fit temperatures of the bremsstrahlung continuum. Structures concentrated at the outer edges and in part of the center show a significantly higher temperature than the rest of the remnant. As shown in Figures 2 and 3, these regions show little evidence of line emission and are correlated with anomalously high absorption column values and with the high energy (4-6 keV) continuum-dominated filaments in Figure 1. There appears to be some genuine elevation of the absorption column in the western region of the remnant, where there is evidence that the remnant is obscured by a molecular cloud[31]. At the outermost edges, the filaments have been associated with the outer shock.[32]. Collectively,

these clues suggest that the model used for the first phase of the analysis is inappropriate in the anomalously high temperature regions because the emission is nonthermal. While some of the high energy X-ray emission (10-60 keV)[33] from Cas A may be produced by nonthermal bremsstrahlung [34]-[36], there is general agreement that the X-ray emission observed from forward-shock filaments is produced by synchrotron emission. Therefore, in Phase 2, we fit the spectra of regions identified by this method with a model composed of realistic synchrotron emission, an absorption column, and a background spectrum.

Creating a cut-off frequency map

Having found a means to identify the regions dominated by nonthermal emission in a remnant whose X-ray emission is globally dominated by thermal emission, we studied the properties of particle acceleration. We used the kT results to pick 10,857 regions—the top 10% of fitted temperatures ($kT > 2.6$ keV). This criterion clearly selected areas centered on and fully containing the outer filaments but not excessive surrounding areas or isolated peaks. Since the fit cut-off frequencies span a range of two orders of magnitude, we believe we found all of the regions of interest without introducing selection effects in the distribution of detected cut-offs.

Our group developed a synchrotron spectrum model in which the effects of spectral “curvature” from the back-pressure of the accelerated cosmic rays are modelled using an electron spectrum whose spectral index is a linear function of the logarithm of the momentum.[37]. The core of the model is the electron distribution function,

$$\frac{dn}{dp} = A_e \left(\frac{pc}{\text{GeV}}\right)^{-\Gamma+a \log_{10}\left(\frac{pc}{\text{GeV}}\right)} e^{-(\text{GeV}-pc)/\epsilon} \quad (1)$$

in which n is the electron number density, c is the speed of light, $p = \gamma mv$ with m the electron mass and v the velocity of a particle, A_e is the number density at $p = 1$ GeV/ c , Γ is the differential spectral index at $p = 1$ GeV/ c , ϵ is the exponential cut-off (maximum) energy, and a is the spectral “curvature.” The parameters of the synchrotron model are the normalization N_s (a function of A_e , distance, and the emitting volume), the total magnetic field B_{tot} , Γ , a , and ϵ .

The cut-off energy ϵ , the normalization of the spectrum and the value of an interstellar absorption column were allowed to be free parameters. We froze the curvature parameter to a value of 0.06 based on fits to radio and infrared synchrotron data for selected regions of Cas A[38]. A value

of $a = 0.05$ was obtained by our group in fits to SN1006[39]. As there are no published values for the radio spectral index of Cas A at the outer shocks, which are at the edge of a diffuse plateau of radio emission, we set $\Gamma = 2.54$, using the average radio spectral index for the entire remnant.[40] Comparison with the index in the plateau region just inside the outer X-ray filaments from unpublished radio spectral index maps suggests this value is reasonable. Small variations in the value of Γ did not significantly affect our final results. Changing the value of Γ by ± 0.1 changed the cut-off frequencies to values within our confidence limits and preserved overall trends.

Some assume the widths of the filaments are limited by synchrotron losses and estimate the strength of the magnetic field in the filaments of Cas A to be $\approx 100 \mu\text{G}$ [36] to $\approx 500 \mu\text{G}$ [41]. Others argue the sizes of the filaments in SNRs are determined by the widths of regions of enhanced magnetic fields at the forward shock, limited by strong turbulent damping of the field to physical sizes of order $10^{16} - 10^{17} \text{ cm}$ [42]. This range corresponds to 0.2 to $2''$ at the distance of Cas A, similar in size to the observed width. The maximum frequency of emission from electrons is related to the maximum energy and the magnetic field as

$$\nu_c = 1.26 \times 10^{16} \left(\frac{\epsilon}{10 \text{ TeV}} \right)^2 \left(\frac{B_{\text{tot}}}{10 \mu\text{G}} \right) \text{Hz}. \quad (2)$$

It may not be possible to uniquely determine ϵ and B_{tot} based on solely on analyses of the X-ray spectra. Therefore, we froze $B_{\text{tot}} = 1000 \mu\text{G}$ (the “equipartition value” for Cas A[33]). As a result, the cut-off energy itself is not well determined, but the cut-off frequency is well determined by the X-ray data.

We present our map of ν_c in Figure 4. Cut-off frequencies in the forward shock vary at least from $5 \times 10^{16} \text{ Hz}$ to $9 \times 10^{17} \text{ Hz}$. The 90% confidence intervals have been computed for all of the cut-off frequencies. The average uncertainties range from about $\pm 20\%$ at $5 \times 10^{16} \text{ Hz}$ to $\pm 40\%$ at $9 \times 10^{17} \text{ Hz}$. Therefore, the cut-off energy and/or the magnetic field vary considerably from one region to another. Variations in the cut-off frequency have been reported for a few other remnants[26],[43]-[45]. The spectrum of a $2'' \times 2''$ region along the shock in the northeast is shown in Figure 5. This region has the highest cut-off frequency ($9 \times 10^{17} \text{ Hz}$).

Constraining the electron diffusion coefficient

As recently reviewed by Vink[46], some analyses are based on the assumption that particle acceleration is efficient: the particle diffusion coefficient is

as small as the Bohm limit[47][48]. Here, we use the spectral results to constrain the efficiency of acceleration of the highest energy electrons at each location dominated by synchrotron radiation.

Assuming that electrons at the cut-off energy cannot experience synchrotron losses in excess of accelerative gains in one cycle through the shock, one can derive an upper limit on the ratio of the electron diffusion coefficient to the Bohm coefficient.[39]. The ratio is a function of the cut-off frequency, the shock velocity u_1 and the compression ratio r . At $E = \epsilon$, $\kappa_B = \epsilon/3eB$ in MKSA and

$$\frac{\bar{\kappa}}{\kappa_B} \leq \frac{9\epsilon_0 mc}{2e^2} \frac{f u_1^2}{\nu_c \sin \theta} \quad (3)$$

$$= 2.08 \left(\frac{f}{0.15} \right) \left(\frac{u_1}{5000 \text{ km s}^{-1}} \right)^2 \left(\frac{\nu_c}{9 \times 10^{17} \text{ Hz}} \right)^{-1}. \quad (4)$$

Here ϵ_0 is the permittivity of free space, and $f = (r - 1)/((r)(r + 1))$.

To constrain the electron acceleration efficiency, we used a value of 5000 km/s for the shock velocity of Cas A[49], and assumed the case of a strong, unmodified shock ($f = 0.15, r = 4$). For the highest cut-off frequencies on the outer shock of Cas A, we obtained $\bar{\kappa}/\kappa_B = 2.1_{-0.7}^{+0.9}$. The variations on the outer rim range from 0.5 to 9×10^{17} Hz, corresponding to $\bar{\kappa}/\kappa_B \sim 36$ to 2. Our upper limits are smallest in certain parts of the north, northeast, and southeast shocks, strongly suggesting efficient particle acceleration occurs in at least these regions.

Conclusions

We developed a method to analyze the emission from extended X-ray sources. We combined multiple data sets retaining pointing-specific calibrations and backgrounds, automated spectral extraction, and fully exploited the spatial and spectral capabilities of *Chandra*. Analyzing the emission from the young Cassiopeia A supernova remnant, we discovered the apparent bremsstrahlung temperature (kT) of regions can be used to identify individual regions which are dominated by nonthermal emission in a SNR globally dominated by thermal emission. For Cas A, we found that the synchrotron emission is clearly correlated with the forward shock, as well as some areas in the center, which may or may not be the forward shock seen in projection. Fitting the nonthermally dominated regions with a synchrotron model, we mapped the cut-off frequency of the synchrotron spectrum associated with

the highest energy electrons accelerated in the forward shock. From the cut-off frequency and shock velocity, we constrained the efficiency of the acceleration of cosmic-ray electrons.

We present the first map of the upper limits on the particle diffusion coefficients in a SNR. Our results suggest that at least in several locations, acceleration occurs nearly as fast as theoretically possible (the Bohm limit). In fact, electrons could also be diffusing in the Bohm limit in other parts of the shock if the shock velocity is lower; if the compression ratio is greater than 4—an enhancement quite possible in a modified shock; or if a process other than synchrotron radiation limits the maximum energy. TeV γ -rays have been detected from Cas A [16][17]. Modeling suggests these could be formed either by the prompt decay of π^0 's created in collisions of cosmic-ray protons accelerated in the SNR with ambient gas; or, by inverse-Compton scattering of cosmic microwave background photons off of the accelerated electrons. Although TeV telescopes cannot yet localize the γ -ray source position with arcsecond accuracy, or determine unambiguously the fraction of π^0 and inverse-Compton produced γ -rays from the spectrum, the expectation that cosmic-ray electrons and protons are accelerated together means that electron synchrotron emission is an important tracer of the particle acceleration. Detailed maps of the X-ray synchrotron emission, such as those we created with *Chandra*, are rapidly improving our understanding of the big picture of cosmic-ray acceleration in SNRs.

Acknowledgements

MDS and GEA thank Tracey Delaney and Lawrence Rudnick for sharing unpublished radio spectral index data of Cas A to help us in determining a reasonable choice of Γ for the forward shock. This work was supported in part by NASA LTSA grant NAG5-9237 and the Five College Astronomy Department Fellowship program.

References

- [1] Baade, W., & Zwicky, F. Cosmic rays from super-novae. *Proc. Nat. Acad. Sci.* **20**, 5, 259-263 (1934).
- [2] Ginzburg V. L. & Syrovatskii, S. I. *The Origin of Cosmic Rays*, New York: Gordon and Breach (1969).

- [3] Krymskii, G. F. A regular mechanism for the acceleration of charged particles on the front of a shock wave. *Akademiia Nauk SSSR Doklady* **234**, 1306-1308 (1977).
- [4] Bell, A. R. The acceleration of cosmic rays in shock fronts – I. *Mon. Not. R. astr. Soc.* **182**, 147-156 (1978).
- [5] Bell, A. R. The acceleration of cosmic rays in shock fronts – II. *Mon. Not. R. astr. Soc.* **182**, 443-455 (1978).
- [6] Blandford, R. D., & Ostriker, J. P. Particle acceleration by astrophysical shocks. *Astrophys. J.* **221**, L29-L32 (1978).
- [7] Drury, L. On Particle Acceleration in Supernova Remnants. *Space Sci. Rev.* **36**, 57-60 (1983).
- [8] Jones, F. C., & Ellison, D. C. The Plasma Physics of Shock Acceleration. *Space Sci. Rev.* **58**, 259-346 (1991).
- [9] Reynolds, S.P. Models of synchrotron X-rays from shell supernova remnants. *Astrophys. J.* **493**, 375-396 (1998).
- [10] Ellison, D. C., Berezhko, E. G., & Baring, M. G. Nonlinear shock acceleration and photon emission in supernova remnants. *Astrophys. J.* **540**, 292-307 (2000).
- [11] Biermann, P. L., & Sigl, G. Introduction to Cosmic Rays. *LNP Vol. 576: Physics and Astrophysics of Ultra-High-Energy Cosmic Rays*, **576**, 1-26 (2001).
- [12] Baring, M. G., Ellison, D. C., Reynolds, P. S., Grenier, I. A., & Goret, P. Radio to gamma-ray emission from shell-type supernova remnants: predictions from nonlinear shock acceleration models. *Astrophys. J.* **513**, 311-338 (1999).
- [13] Ellison, D. C., & Cassam-Chenai, G. Radio and X-ray profiles in supernova remnants undergoing efficient cosmic-ray production. *Astrophys. J.* **632**, 920-931 (2005).
- [14] Ellison, D. C., Decourchelle, A., & Ballet, J. Nonlinear particle acceleration at reverse shocks in supernova remnants. *Astron. Astrophys.* **429**, 569-580 (2005).

- [15] Bell, A. R. Cosmic ray acceleration to very high energy through the non-linear amplification by cosmic rays of the seed magnetic field. *Mon. Not. R. astr. Soc.* **321**, 433-438 (2005).
- [16] Pühlhofer, G., Völk, H., Wiedner, C. A., for the HEGRA Collaboration. Observations of the supernova remnants Cas-A and Tycho with the HEGRA stereoscopic IACT system. *Proc. 26th Intl. Cosmic Ray Conf* **3**, 492-495 (1999).
- [17] Aharonian, F., et al. Evidence for TeV gamma ray emission from Cassiopeia A. *Astron. Astrophys.* **370**, 112-120 (2001).
- [18] Muraishi, H., et al. Evidence for TeV gamma-ray emission from the shell type SNR RX J1713.7-3946. *Astron. Astrophys.* **354**, L57-L61 (2000).
- [19] Enomoto, R., et al. The acceleration of cosmic-ray protons in the supernova remnant RX J1713.7-3946. *Nature.* **416**, 823-826 (2002).
- [20] Aharonian, F. A. et al. High-energy particle acceleration in the shell of a supernova remnant. *Nature* **432**, 75-77 (2004).
- [21] Aharonian, F., et al. Detection of TeV γ -ray emission from the shell-type supernova remnant RX J0852.0-4622 with HESS. *Astron. Astrophys.* **437**, L7-L10 (2005).
- [22] Katagiri, H., et al. Detection of gamma rays around 1 TeV from RX J0852.0-4622 by Cangaroo-II. *Astrophys. J.* **619**, L163-L166 (2005).
- [23] Aharonian, F., et al. Very high energy gamma rays from the composite SNR G 0.9+0.1. *Astron. Astrophys.* **432**, L25-L29 (2005).
- [24] Koyama, K., et al. Evidence for shock acceleration of high energy electrons in the supernova remnant SN:1006. *Nature* **378**, 6554, 255-256 (1995).
- [25] Weisskopf, M. C., et al. An Overview of the performance and scientific results from the *Chandra X-ray Observatory*. *Pub. Astr. Soc. Pac.* **114**, 1-24 (2002).
- [26] Lazendic, J. S., et al. A high resolution study of nonthermal radio and X-ray emission from supernova remnant G347.3-0.5. *Astrophys. J.* **602**, 271-285 (2004).

- [27] Warren, J. et al. Cosmic-ray acceleration at the forward shock in Tycho's supernova remnant: evidence from *Chandra* X-ray observations. *Astrophys. J.* **634**, 376-389 (2000).
- [28] Houck, J. C., and Denicola, L. A. ISIS: An Interactive Spectral Interpretation System for high resolution X-ray spectroscopy. *ASP Conf. Ser. 216: Astronomical Data Analysis Software and Systems IX*, **216**, 591-594 (2000). (available at <http://space.mit.edu/ASC/ISIS/>)
- [29] Hwang, U., et al. A million second *Chandra* view of Cassiopeia A. *Astrophys. J.* **615**, L117-L120 (2004).
- [30] Davis, J. E., Houck, J. C., Allen, G. E., and Stage, M. D. Analyzing the Cas A megasecond in less than a megasecond. *ASP Conf. Ser. 347: Astronomical Data Analysis Software and Systems XIV*, **347**, p2.3-1-2.3-4 (2005).
- [31] Keohane, J.W., Rudnick, L., & Anderson, M.C. A comparison of X-ray and radio emission from the supernova remnant Cassiopeia A. *Astrophys. J.* **466**, 309-316 (1996).
- [32] Gotthelf, E., Koralesky, B., Rudnick, L., Jones, T. W., Hwang, U., & Petre, R. *Chandra* detection of the forward and reverse shocks in Cassiopeia A. *Astrophys. J.* **552**, L39-L43 (2001).
- [33] Allen, G. E., et al. Evidence of X-ray synchrotron emission from electrons accelerated to 40 TeV in the supernova remnant Cassiopeia A. *Astrophys. J.* **497**, L97-L100 (1997).
- [34] Laming, J. M. Accelerated electrons in Cassiopeia A: an explanation for the hard X-ray tail. *Astrophys. J.* **546**, 1149-1158 (2001).
- [35] Bleeker, J. A. M. et al. Cassiopeia A: On the origin of the hard X-ray continuum and the implication of the observed O_{VIII} Ly- α /Ly- β distribution. *Astron. Astrophys.* **365**, L225-L230 (2001).
- [36] Vink, J., & Laming, J. M. On the magnetic fields and particle acceleration in Cassiopeia A. *Astrophys. J.* **584**, 758-769 (2003).
- [37] Houck, J. C., & Allen, G. E. Models for nonthermal photon spectra. *Astrophys. J.* in press (2006) (also available at <http://xxx.lanl.gov/archive/astro-ph/0607574>).

- [38] Jones, T. J., Rudnick, L., DeLaney, T., & Bowden, J. The identification of infrared synchrotron radiation from Cassiopeia A. *Astrophys. J.* **587**, 227-234 (2003).
- [39] Allen, G. E., Houck, J. C., and Sturmer, S. J. Evidence of a curved cosmic-ray electron spectrum in the supernova remnant SN 1006. *Astrophys. J.* submitted (2006).
- [40] Baars, J. W. M., Genzel, R., Pauliny-Toth, I. I. K., & Witzel, A. The absolute spectrum of Cas A; an accurate flux density scale and a set of secondary calibrators. *Astron. Astrophys.* **61**, 99-106 (1977).
- [41] Berezhko, E. G. & Völk, H. J. Direct evidence of efficient cosmic ray acceleration and magnetic field amplification in Cassiopeia A. *Astron. Astrophys.* **419**, L27-L30 (2004).
- [42] Pohl, M., Yan, H., & Lazarian, A. Magnetically limited X-ray filaments in young supernova remnants. *Astrophys. J.* **626**, L101-104 (2005).
- [43] Pannuti, T. G., Allen, G. E., Houck, J. C., & Sturmer, S. J. *RXTE*, *ROSAT*, and *ASCA* observations of G347.3-0.5 (RX J1713.7-3946): probing cosmic-ray acceleration by a galactic shell-type supernova remnant. *Astrophys. J.* **593**, 377-392 (2003).
- [44] Bamba, A., Yamazaki, R., Ueno, M., & Koyama, K. Small-scale structure of the SN 1006 shock with *Chandra* observations. *Astrophys. J.* **589**, 827-837 (2003).
- [45] Rothenflug, R. et al. Geometry of the non-thermal emission in SN 1006: azimuthal variations of cosmic-ray acceleration. *Astron. Astrophys.* **425**, 121-131 (2004).
- [46] Vink, J. X-ray high resolution and imaging spectroscopy of supernova remnants. *Proc. of the Symp: The X-Ray Universe*, in press (2006).
- [47] Völk, H. J., Berezhko, E. G., Ksenofontov, L. T. K. Magnetic field amplification in Tycho and other shell-type supernova remnants *Astron. Astrophys.* **433**, 229-240 (2005).
- [48] Bamba, A., Yamazaki, R., Hiraga, J. S. A spatial and spectral study of nonthermal filaments in historical supernova remnants: observational results with *Chandra*. *Astrophys. J.* **621**, 793-802 (2005).

- [49] DeLaney, T., & Rudnick, L. The first measurement of Cassiopeia A's forward shock expansion rate. *Astrophys. J.* **589**, 818-826 (2003).

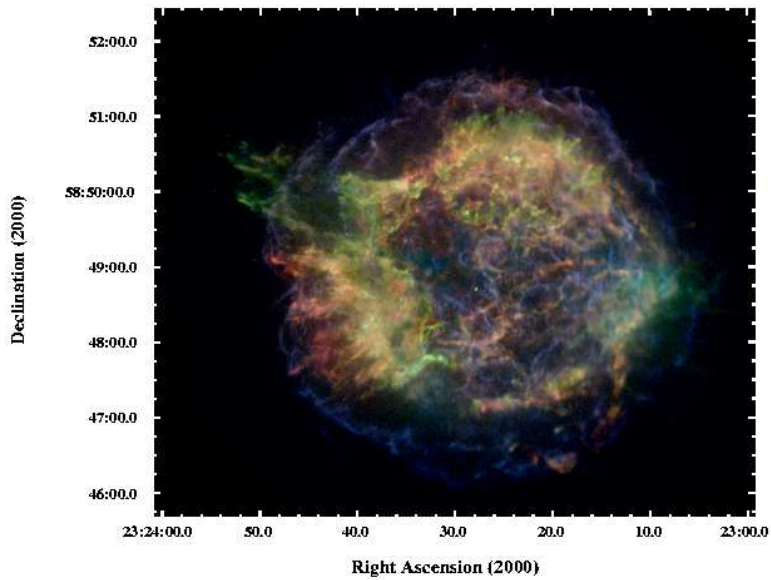


Figure 1: The Cassiopeia A supernova remnant as observed by *Chandra*. Red: 0.5 - 1.5 keV: O-K, Ne-K, Mg-K, and Fe-L emission. Green: 1.5-2.5 keV: Si-K and S-K. Blue: 4.0-6.0 keV: high energy continuum (some energy ranges have been excluded, including Fe-K). This energy-colored photon counts image was created from 1.08 Ms of ACIS data. The colors are individually log-scaled to bring out the fine structure in the remnant. The bulk of the X-ray photons are thermal radiation from the ejecta which has passed through the hot reverse shock. Note in particular the wispy blue filamentary structure of the forward shock, dominated by high-energy synchrotron emission from electrons accelerated at the forward shock.

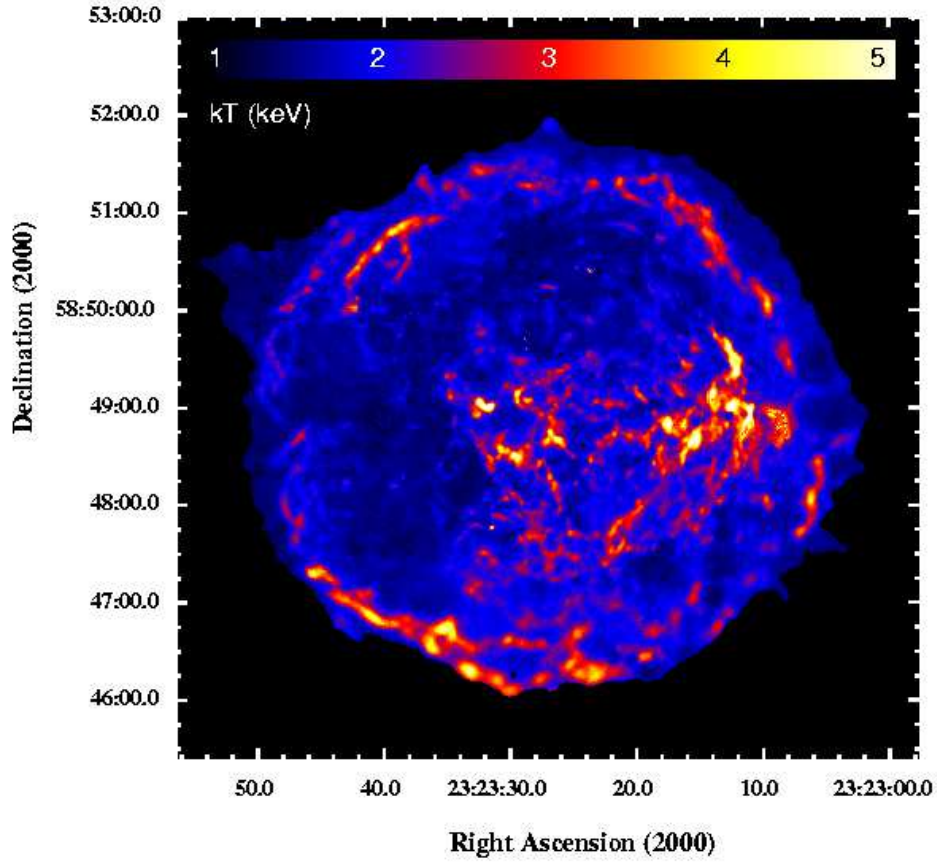


Figure 2: Cas A bremsstrahlung temperature map. The image is of the fit bremsstrahlung continuum from the Phase 1 analysis of the remnant. We fit the spectrum of 104,393 regions with a model that includes 15 Gaussian lines, interstellar absorption, and a thermal bremsstrahlung continuum. Note the correlation between the high-temperature features in this image and the blue, high-energy continuum-dominated filaments in Figure 1. The anomalously high temperatures in this image indicate nonthermal emission in the SNR, which is likely synchrotron radiation from electrons accelerated to TeV energies.

Thermal and Continuum dominated regions

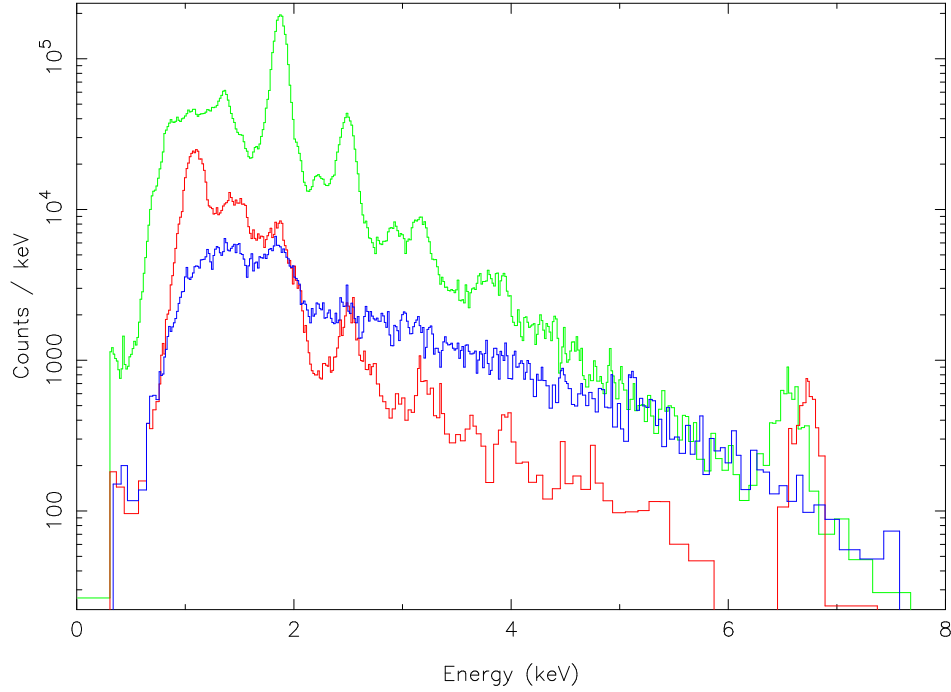


Figure 3: Comparison of a continuum-dominated spectrum (blue) from a $2''$ by $2''$ region on the northeast shock ($\alpha=23:23:42.2$, $\delta=58:50:26.4$) shows it has a different spectral shape than spectra from same-sized regions dominated by line emission (Si, S, Fe, O, Ne, Mg, Ar, Ca). The green spectrum is taken from a region in the northern lobe ($\alpha=23:23:52.1$, $\delta=58:50:33.3$) featuring strong K-line emission from silicon and sulfur. The red spectrum is from the fingerlike projections in the southeast lobe ($\alpha=23:23:44.0$, $\delta=58:48:04.7$) dominated by iron L and K emission. The exposure time is 1.08 Ms, and for display the spectra are binned to contain at least 10 counts per bin.

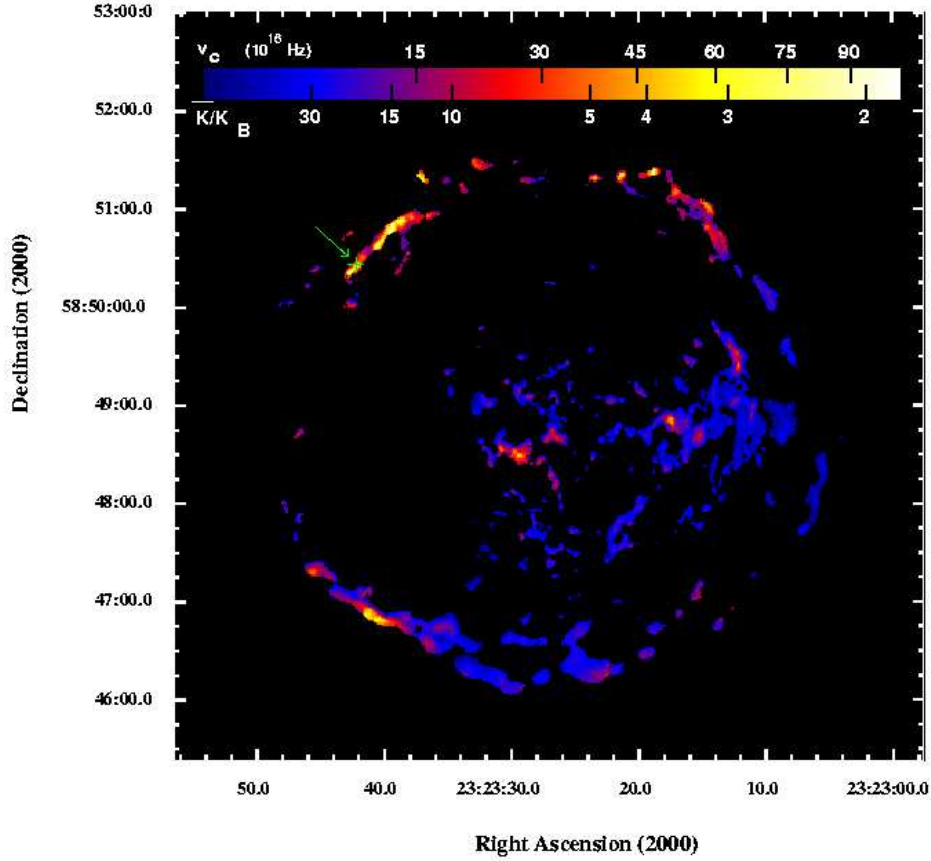


Figure 4: Synchrotron cut-off frequencies and upper limits on the electron diffusion coefficient in the Cassiopeia A supernova remnant. A synchrotron model which includes curvature in the electron distribution spectrum was used to fit the spectra of 10,857 regions identified from the kT map as likely sites of nonthermal emission (see Figure 5) because they have anomalously high bremsstrahlung temperatures (i.e. $kT > 2.6$ keV, Figure 2). The fitted cut-off frequencies and estimates of the shock velocity and compression ratio are used to determine an upper limit on the ratio of the electron diffusion coefficient ($\bar{\kappa}$) to the Bohm diffusion coefficient (κ_B). The highest fit cutoff value occurs at the $2'' \times 2''$ region indicated by the green cross and arrow; the fit is shown in Figure 5. A ratio close to 1, as seen in the yellow and white regions of the map, indicates that acceleration must be occurring almost as fast as theoretically possible (in the Bohm limit).

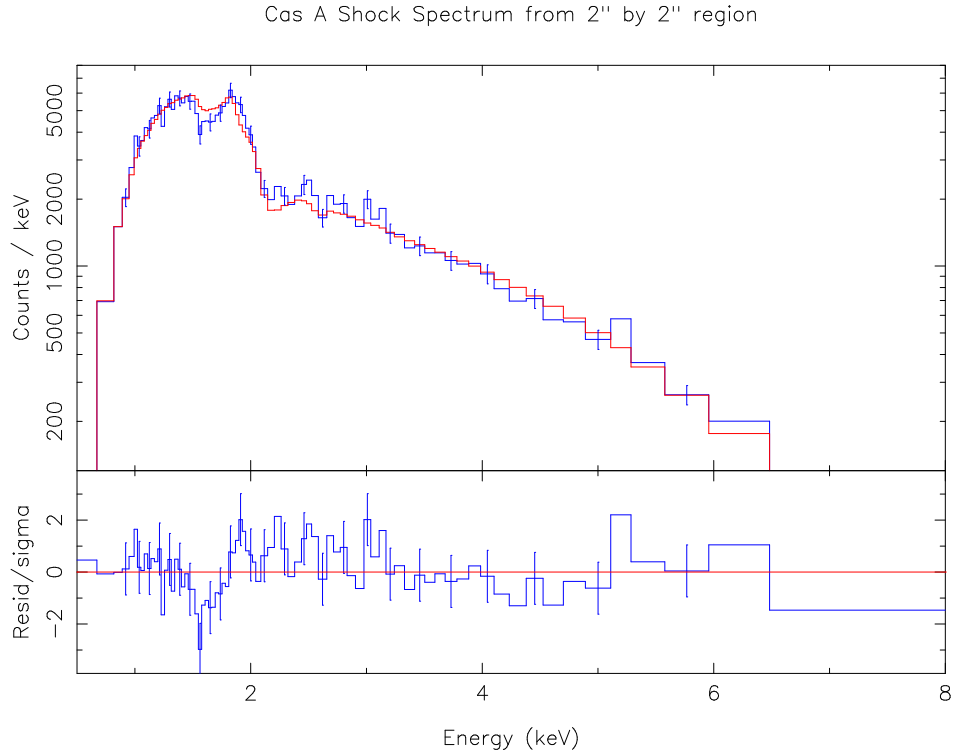


Figure 5: The nonthermal continuum spectrum of the 2'' by 2'' region on the northeast shock ($\alpha=23:23:42.2$, $\delta = 58:50:26.4$) which shows the highest cut-off frequency, 9×10^{17} Hz. The blue histogram is the combined data; the red histogram is the model plus combined background. The apparent (thermal) structure between 1 and 3 keV is primarily background. Only every third error bar has been plotted to improve clarity. The exposure time is 1.08 Msec and for fitting the spectrum has been binned to contain a minimum of 100 counts per bin.